Dynamics of Bacteriorhodopsin in the Dark-Adapted State from Solution NMR

Kooijman, Laurens ; Schuster, Matthias ; Baumann, Christian ; Jurt, Simon ; Löhr, Frank ; Fürtig, Boris ; Güntert, Peter ; Zerbe, Oliver

Abstract: To achieve efficient proton pumping in the light-driven proton pump bacteriorhodopsin, the protein must be tightly coupled to the retinal to rapidly convert retinal isomerization into protein structural rearrangements. Methyl group dynamics of bR embedded in lipid nanodiscs were determined in the dark-adapted state, and were found to be mostly well-ordered at the cytosolic side. Methyl groups in the M145A mutant of bR, which displays only 10% residual proton pumping activity, are less well ordered suggesting a link between side chain dynamics on the cytosolic side of the bR cavity and proton pumping activity. In addition, slow conformational exchange, attributed to low frequency motions of aromatic rings, was indirectly observed for residues on the extracellular side of the bR cavity. This may be related to reorganization of the water network. These observations provide a detailed picture of previously undescribed equilibrium dynamics on different time scales for ground-state bR.

DOI: https://doi.org/10.1002/anie.202004393

10.1002/anie.202004393

WILEY-VCH

RESEARCH ARTICLE

Dynamics of Bacteriorhodopsin in the Dark-Adapted State from Solution NMR

Laurens Kooijman[a], Matthias Schuster[a], Christian Baumann[a], Simon Jurt[a], Frank Löhr[b], Boris Fürtig[c], Peter Güntert[b,d] and Oliver Zerbe[a,]*

[a] Dipl. Chem. L. Kooijman, Dr. M. Schuster, Msc. Biochem. C. Baumann, S. Jurt, Prof. Dr. O. Zerbe
Department of Chemistry, University of Zurich
Winterthurerstrasse 190, CH-8057 Zurich (Switzerland)
E-mail: oliver.zerbe@chem.uzh.ch
[b] Dr. F. Löhr, Prof. Dr. P. Güntert
Institute of Biophysical Chemistry, Center for Biomolecular Magnetic Resonance, Goethe University Frankfurt
Max-von-Laue-Straße 9, 60438 Frankfurt am Main (Germany)
[c] Dr. B. Fürtig
Institute of Organic Chemistry and Chemical Biology, Goethe University Frankfurt
Max-von-Laue-Straße 7, 60438 Frankfurt am Main (Germany)
[d] Prof. Dr. P. Güntert
Laboratory of Physical Chemistry, ETH Zürich
Vladimir-Prelog-Weg 2, 8093 Zurich (Switzerland)

Supporting information for this article is given via a link at the end of the document.

Abstract: To achieve efficient proton pumping in the light-driven proton pump bacteriorhodopsin, the protein must be tightly coupled to the retinal to rapidly convert retinal isomerization into protein structural rearrangements. Methyl group dynamics of bR embedded in lipid nanodiscs were determined in the dark-adapted state, and were found to be mostly well-ordered at the cytosolic side. Methyl groups in the M145A mutant of bR, which displays only 10% residual proton pumping activity, are less well ordered suggesting a link between side chain dynamics on the cytosolic side of the bR cavity and proton pumping activity. In addition, slow conformational exchange, attributed to low frequency motions of aromatic rings, was indirectly observed for residues on the extracellular side of the bR cavity. This may be related to reorganization of the water network. These observations provide a detailed picture of previously undescribed equilibrium dynamics on different time scales for ground-state bR.

Introduction

7-transmembrane (7-TM) helical proteins are found in all domains of life, from microbial rhodopsins to G-protein-coupled receptors encountered in animals and most other eukaryotes. The archaeal proton pump bacteriorhodopsin (bR) mediates photosynthesis in halobacteria, and presents a prototypical example of 7-TM proteins [1–3] that has been studied intensively using a variety of biophysical methods.[1,4–11] Photoactivation of bR results in isomerization of the centrally bound all-*trans* retinal to the 13-*cis*,15-*anti* species, and proceeds through a series of well-characterized intermediates until the light-adapted (all-trans) state is formed again. The kinetics of the photocycle intermediates of retinal and the protein response were determined using time-resolved infrared experiments.[12,13] In particular, carbonyl vibration frequencies were utilized to determine the protonation state of carboxyl groups involved in transferring the proton from carboxyl groups to the Schiff base and back during the proton pumping cycle in order to understand the proton-transfer pathway. Recently, time-resolved free-electron laser or serial synchrotron [14] crystallography provided unprecedented structural details of retinal isomerization [15] and the protein response [16,17] following laser-flash induced retinal perturbation.

Despite the enormous amount of spectroscopic studies aimed at describing the photoactivation and proton-translocation process of bacteriorhodopsin in great detail, surprisingly little is known about the equilibrium dynamics in the dark. A particularly interesting question is how bR is structurally and dynamically prepared to respond to photons with very high overall quantum yields [18,19] and rate constants for formation of the first intermediate in the photocycle in the order of 10^5 s^{-1}.[20] To achieve such efficiencies, retinal must be tightly coupled to the protein so that its isomerization can very rapidly trigger protein conformational changes. Therefore, it is of great interest to not only study effects of perturbation of bR by photons but to also inspect the dark-adapted state in more detail. In that state retinal exists in a 4:6 ratio of the all-*trans* to 13-*cis*,15-*syn* retinal isomers (Fig. 1A) [21] and only the all-*trans* form can directly enter the photocycle. At the end of the photocycle all-*trans* retinal is formed again, which can thermally equilibrate to the 13-*cis*,15-*syn* isomer. [22]

It has been demonstrated by Khorana and coworkers that in the dark mutants of the retinal-lining pocket populate the two retinal isomers to different extents,[23] display different proton-pumping activities, and are characterized by different kinetics of the photocycle. We hypothesized that dynamics of residues, and in particular of their side chains, control the coupling of retinal to the protein and are important for the kinetics and outcomes of photoactivation. Therefore, we probed methyl group dynamics of

bR in the thermodynamically equilibrated dark-adapted state using solution NMR techniques.

NMR had previously been used to determine the retinal binding mode in the dark-adapted state by solution [24] and solid-state methods.[21,25,26] In our dynamics study we used nanodiscs that present planar lipid surfaces similar to biological membranes. Since lipid curvature and planar pressure fine-tune the architecture of 7-TM membrane proteins [27–30] we believe that the more challenging spectroscopy with nanodiscs was justified.[31–36] To cope with the increased size of the system, we recently developed a protocol for resonance assignments in the absence of extensive mutagenesis.[37] It uses the program FLYA, [38,39] which combines information from NMR experiment utilizing scalar or dipolar couplings in combination with structural data to form assignments. The new approach included factors such as proximity to water and lipid molecules, as well as biochemical information from differential isotope labeling. Interestingly, many signals from residues in the extracellular half of bR were absent, likely due to intermediate conformational exchange. Two sets of peaks were present in the spectra arising from the two all-*trans*,15-*anti* and 13-*cis*,15-*syn* isomeric states of retinal. [37]

In this work we now compare spectra in the dark to those recorded upon laser illumination to assign which of the two sets of peaks belong to the light-adapted all-*trans*,15-*anti* state. The availability of methyl group assignments allowed us to measure site-specific methyl group relaxation rates and to compute order parameters from the NMR data. The relaxation data revealed regions of increased or decreased methyl group mobility in bR.

Moreover, we determined methyl group dynamics of the M145A mutant, which has only 10% of the wild-type proton pumping activity, and compared methyl order parameters of this mutant with those from the wildtype protein. We found that methyl groups in wt-bR are more rigid than in the M145A mutant, thereby enabling more efficient coupling of retinal to wt-bR. Moreover, we detected a second, much slower, conformational exchange process, possibly related to a reorientation of aromatic rings of Trp residues, which we attribute to the reorganization of the water network.

Results and Discussion

Biosynthesis and resonance assignments

The apo-protein bacterio-opsin (bO) was expressed in the form of a C-terminal fusion to Mistic in E. coli [40] into inclusion bodies (Fig. S1). After cleavage of the Mistic tag, addition of retinal and of lipids, and removal of detergent using BioBeads,[41] the resulting bacteriorhodopsin (bR) was incorporated into the MSPΔH5 variant of the membrane scaffold protein (MSP).[42] bR was generally perdeuterated, with ILV sidechains being [^{12}C,^{2}H] and one of the two methyl groups (in Ile the δ1) being [^{13}C,^{1}H] labeled in a non-stereospecific fashion using α-ketoisovaleric and α-ketobutyric acid as precursors. In one wt-bR sample and in M145A-bR the Met methyl group was [^{13}C,^{1}H] labeled while the rest of the sidechain contained [^{12}C,^{1}H] by supplementing the expression medium with appropriately labeled methionine. The typical purple color from the chromophore (Fig. S2) and the characteristic shift of the absorption maximum between dark- (550 nm) and light-adapted (558 nm) bacteriorhodopsin indicated correct refolding (Fig. S3). The incorporation, purification, and separation of bR trimers in high yields into larger MSP1E3D1 nanodiscs,[43] from detergent refolded bR as well as the direct refolding with bO, unfortunately failed.

To compensate for problems associated with resonance assignments of large membrane proteins we developed a protocol that incorporates topological, structural, and biochemical information. The production of wt-bR in DMPG nanodiscs and its resonance assignment is described in Kooijman et al. [37] Overall, we assigned 156 backbone amide groups (62%) and 95 methyl groups (59% of Ala, Ile(δ1), Leu(δ1/2), Val(γ1/2)). Additionally we were able to identify the amino acid type of all methyl groups using HMCM-CG/CB/CA type experiments. [37,44] The unassigned residues are mostly located in the extracellular halves of the helices, the extracellular loops, and the entirety of helix 5. Since we assigned the vast majority of the observable peaks, this suggests that these parts of the protein undergo intermediate conformational exchange resulting in peaks that are broadened beyond detection (*vide infra*).

Detection of the two isomeric states of retinal in the dark-adapted state

Duplication of many peaks was observed in [^{15}N,^{1}H]-TROSY and methyl [^{13}C,^{1}H]-TROSY spectra of bR (Fig. 1B) as indicated by the presence of nearly-identical correlations in the 3D spectra. Doubling was noticed for 48 amide and 31 methyl spin systems with combined proton and ^{13}C/^{15}N chemical shift differences, $\left(\Delta\delta_{\mathrm{H}}^2 + \Delta\delta_{\mathrm{N,C}}^2/4\right)^{1/2}$, in [^{15}N,^{1}H]-TROSY and methyl [^{13}C,^{1}H]-TROSY ranging from 0.013 ppm to 0.24 ppm.[37] We noticed that doubling in our initial analysis [37] and attribute this peak doubling to the dark-adaptation of bR, which results in a mixture of all-trans,15-anti and 13-cis,15-syn isomers of retinal.[21] The isomer ratio of all-trans,15-anti:13-cis,15-syn has been determined previously as 1:1.6 by HPLC for retinal extracted from bR,[23] or 1:1.5 by solid-state NMR [21] similar to the 1:1.6 and 1:2.0 ratio measured by us from the average intensity ratio of corresponding peaks in [^{15}N,^{1}H]-TROSY and methyl [^{13}C,^{1}H]-TROSY spectra, respectively. Scherrer and coworkers compared the retinal isomer ratio for the bR trimer in purple membranes and the monomer solubilized in Triton X-100 [45] and concluded that the isomer ratio is very similar in the two environments. Importantly, it was demonstrated that the bR monomer is capable of pumping protons [46] and hence presents the functional unit for the photocycle.[47]

The residues that display peak doubling are spread over the entire protein (Fig. S6). The magnitude of chemical shift differences between the two states shows no correlation with the proximity to retinal or aromatic side chains. Apparently, subtle structural adaptations upon isomerization of the chromophore, not easily detected when comparing the crystal structures of the all-trans (PDB 1M0L) [48] and the 13-cis (1X0S) [49] isomers, are felt throughout the entire protein. The corresponding isomerization is a thermal process with a rate constant on the order of minutes, resulting in peak doublets due to slow exchange on the NMR time-scale.[24] This is corroborated by the absence of exchange peaks in ^{15}N and ^{13}C zz-TROSY experiment recorded with a delay time of 500 ms.

Subsequently, we tested whether illumination could convert the dark-adapted state entirely into the light-adapted state. To this end, we illuminated a bR NMR sample constantly with 53 mW laser power at 488 nm in situ while measuring [^{15}N,^{1}H]- or [^{13}C,^{1}H]-TROSY spectra (Fig. 1). As a result, one of the two corresponding peaks almost completely vanished while the other remained, not

10.1002/anie.202004393

RESEARCH ARTICLE

only demonstrating that the peak duplications arise from the two isomeric retinal forms of bR but also facilitating their respective assignments to the all-trans and 13-cis,15-syn states.
Khorana and coworkers investigated a series of retinal-binding-pocket mutants and discovered that most of them resulted in an altered ratio of the all-trans and 13-cis,15-syn retinal isomers.[23] By retinal extraction the amount of the all-trans state for the M145A mutant was estimated to be 90%. Interestingly, in the M145A mutant duplicated peaks collapse almost completely into single sharp peaks, supporting the view that the peak duplications originate from the presence of two retinal isomers of bR in the dark state (Fig. 1, Fig. S8).

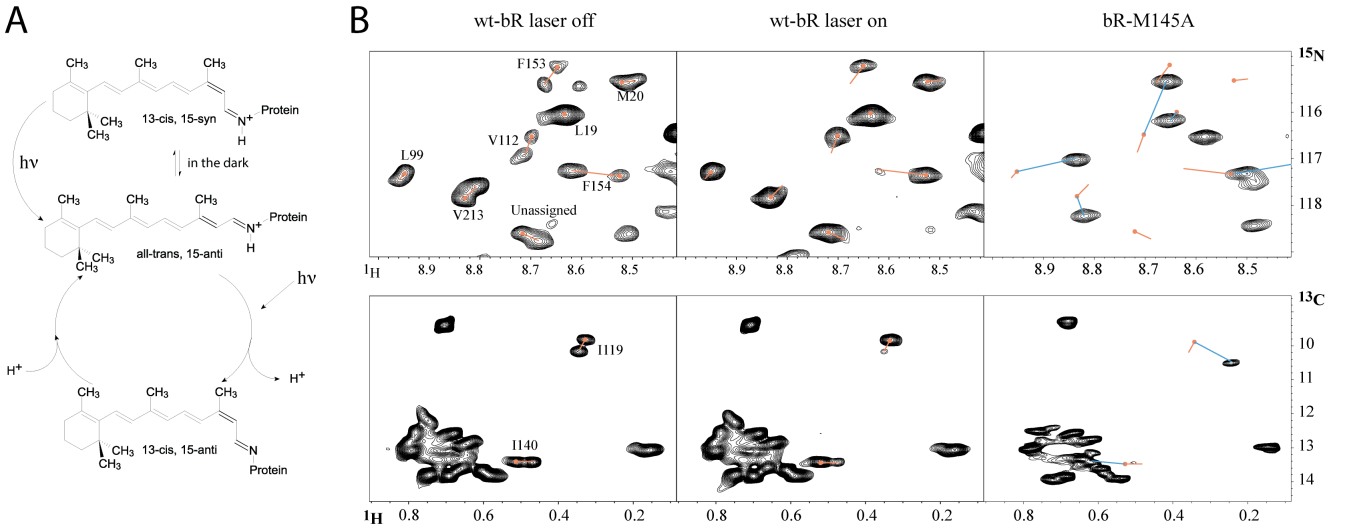

Figure 1. Peak doubling in [^{13}C,^{1}H]- and [^{15}N,^{1}H]-TROSY spectra: **A** Configurations of retinal in the dark-adapted and light-activated states. **B** Representative expansions of spectra showing peak doubling in a well resolved region of the [^{15}N,^{1}H]-TROSY spectrum (top) and in the Ile region of the [^{13}C,^{1}H]-TROSY spectrum (bottom) measured for [(^{13}C-^{1}H-δ-Methyl)-Ile, (^{13}C-^{1}H-δ-Methyl)-Leu, (^{13}C-^{1}H-γ-Methyl)-Val]-wt-bR without (left) and with laser illumination at 488 nm (center) and the [(^{13}C-^{1}H-δ-Methyl)-Ile, (^{13}C-^{1}H-δ-Methyl)-Leu, (^{13}C-^{1}H-γ-Methyl)-Val, (^{13}C-^{1}H-ε-Methyl)-Met]-M145A-bR mutant (no illumination, right). Red dots indicate peak positions in the light-adapted state of wt-bR, connected by orange lines to the corresponding second state in dark-adapted wt-bR, and by blue lines in the right panel to the corresponding peak for the M145A mutant.

Determination of methyl group dynamics

A particular strength of NMR spectroscopy is its capability to quantify protein dynamics. Measuring backbone dynamics of large membrane proteins such as bR embedded in nanodiscs is technically very challenging as the sensitivity of relaxation experiments is unfortunately very low, even when using TROSY-type versions.[50] These experiments are therefore impractical, and peak intensities are often used instead to differentiate degrees of mobility. Methyl labeling presents a promising alternative, in particular for ILV-protonated but otherwise perdeuterated proteins, which display stronger signals with reduced transverse relaxation rates.[51] Membrane proteins usually have a rather uniform distribution of methyl groups so that probes for side chain dynamics exist in most parts of the protein.
To derive S^2 order parameter for bR,[52] we applied triple-quantum based experiments developed by Kay and Tugarinov [52,53] that bypass problems in the interpretation of methyl relaxation data due to the presence of different relaxation pathways. Using the overall correlation time of 50 ns as determined from TRACT experiments,[37] we obtained S^2 order parameter values for 14 Ile, 17 Val and 33 Leu methyl groups of dark-adapted bR (Fig. 2, Fig. S9 and Table S2). Unfortunately, the peaks due to the all-*trans* and 13-*cis*,15-*syn* species could in general not be integrated separately, and hence mostly present averaged values from the two species (Table S1). For 6 methyl groups the chemical shift difference was sufficiently large so that peaks could be reliably integrated separately (Table S4). The difference in S^2 was generally less than 0.07 with the sole exception of Ile-119, which is in close proximity to the retinal. We refrained from conducting experiments in the presence of laser illumination because we were concerned that the illumination might contribute to changes in structure and dynamics of the dark-adapted state.
According to Igumenova et al.,[54] observed S^2 order parameters can be classified into distinct groups, which roughly correspond to the extent to which different rotameric states of the side chain are populated i.e. as flexible (J-class), intermediate motions (α-class), or rigid species (ω-class). The ω-class mainly populates a single rotameric state while J-class methyls jump rapidly through multiple rotameric states. Recently, an additional highly dynamic class has been identified that is only observed in membrane proteins. [55] This J'-class is also populated in bR (Fig. 2A), but only by Ile and Leu residues (Fig. S10). In contrast, no residues belonging to the very rigid ω-class are observed, in agreement with observations in pSRII and OmpW, where only one or three methyl groups populate the ω-class, respectively. [55] Common indicators of dynamics such as side chain packing, B-factors, signal intensities, or secondary chemical shifts do not correlate well with the order parameter (data not shown), an observation that has been previously reported for other (soluble) proteins.[54,56,57]
The majority of methyl groups tend to be clustered in the structure with other methyl groups of similar S^2 order parameters, based on k-means clustering and a network approach. Details of this analysis are reported in the Supp. Mat. Both methods identify up to four clusters that show smaller pairwise order parameter differences than the overall mean (Fig. S18). One cluster

10.1002/anie.202004393

comprises residues in the cytosolic cavity of bR, in which average S^2 order parameters are higher than in the remainder of the protein (Fig. S16 & S17). Interestingly, S^2 for methyl groups of Ile and Leu but not Val residues are weakly correlated to the distance to retinal atoms with highest values observed for those methyl groups that are in proximity to retinal (Fig. S13). In our analysis we also observe that S^2 values tend to be more similar to close methyl groups than to the overall pairwise average (Fig. S12).

Most methyl groups that show fast-dynamics are mainly located on the helix surfaces and on one of the small sides of the TM bundle (helices A/B). While for many residues with duplicated signals good fits could not be obtained from the relaxation experiments, often due to signal overlap, the difference in order parameter for methyl groups, for which both peak pairs were assigned and which resulted in good fits, was mostly only minor. A notable exception is Ile-119, which is inside the retinal binding pocket (Table S4). The Ile-119 methyl group corresponding to the light-adapted state (with retinal in all-trans) displays an order parameter S^2 of 0.49 (more rigid) while the corresponding methyl group from the 13-*cis*,15-*syn* state has an S^2 of 0.37 (less rigid).

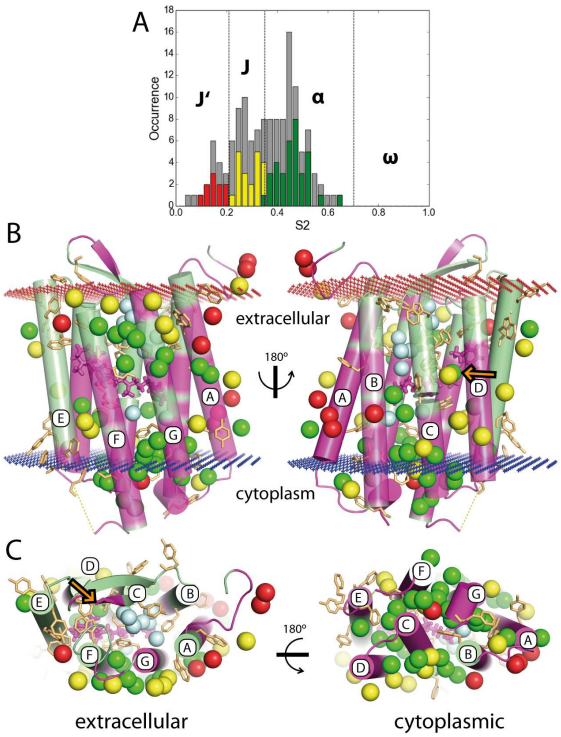

Figure 2. Methyl dynamics of ILV residues in dark-adapted bR. A Histogram of all S^2 values derived from triple-quantum relaxation of methyl groups. Order parameters from assigned residues are highlighted in color. Bands are based on k-means clustering with centers at S^2 = 0.14 (J'), 0.27 (J) and 0.45 (α). **B,C** Locations of methyl carbon atoms shown as spheres in the bR structure with the backbone colored in magenta for assigned residues. Methyl groups are colored according to their classification into the three dynamic ranges, J' (red), J (yellow) and α (green) using the ranges shown in A. TM helices 1 to 7 are denoted as A to F in the structures. Crystallo-graphically-defined water molecules are indicated by blue spheres, the cofactor retinal with the K216 side chain is depicted in thick sticks and aromatic residues are depicted as yellow sticks. The orange arrow indicates the position of I119, the assigned methyl group that is closest to the retinal.

Since Ile-119 packs against retinal (arrow in Fig. 2B), the all-*trans* retinal apparently restricts the Ile-119 δ1 methyl group more than the 13-*cis* retinal.

We also probed for conformational exchange processes using ^{13}C relaxation dispersion experiments. However, dispersion profiles were essentially flat for all residues (data not shown) indicating that conformational exchange processes of methyl groups are either absent or take place on timescales to which the applied methods are insensitive.

Perturbation of the retinal binding pocket

Peak doubling was almost completely absent in M145A bR and the spectral quality was slightly better than for wt-BR. Although the mutated bR shows only 10% of wild-type activity, retinal still absorbs light at 475 nm, resulting in an orange instead of the purple color observed for wt-bR (Fig. S2). Using just 3D ^{15}N-resolved and ^{13}C-resolved [^1H,^1H]-NOESY, HNCA and HNCO spectra we were now able to transfer 89% of the amide and 79% of the methyl assignments from the previously assigned wt-bR to M145A-bR, allowing us to analyze the effect of the mutation on methyl S^2 order parameters, [^{15}N,^1H]-TROSY/[^{13}C,^1H]-HMQC signal intensities and chemical shifts (Fig. 3, Fig. S19).

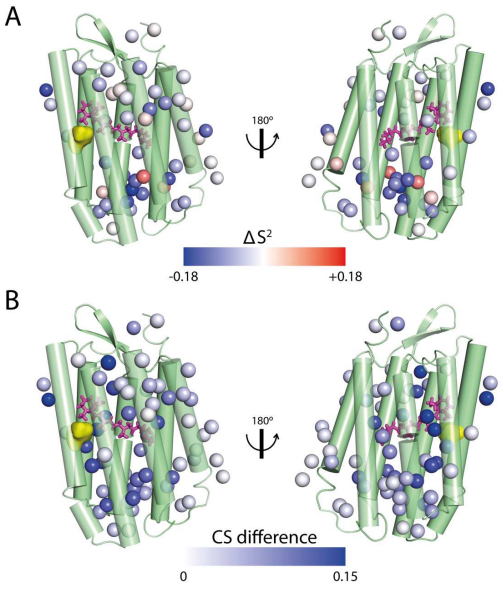

Figure 3. Effect of the M145A mutation on the methyl S^2 order parameter, signal intensity and chemical shift. Each methyl group for which we have data in both wt-bR and M145A is represented by a single sphere with coloring as indicated by the legend. **A** Differences in the S^2 order parameter, $\Delta S^2 = S^2_{\mathrm{M145A}} - S^2_{\mathrm{wt}}$. Negative values of ΔS^2 correspond to methyl groups that become more flexible in M145A-bR. **B** Combined proton and carbon chemical shift, $(\Delta\delta_H^2 + \Delta\delta_C^2/4)^{1/2}$, differences, with the position of doubled peaks in wt-bR averaged.

Chemical shifts of the majority of signals changed only slightly or not at all. The ones that do change significantly are mostly those for which duplicated signals were observed in wt-bR. Changes are localized around the mutation site, but also inside the helix bundle on the intracellular side of bR. Again, we could measure an extensive set of relaxation data for the methyl groups of Ile, Leu and Val residues. For methyl groups in these locations there was a good correlation between S^2 values, chemical shift changes and

signal intensities. A clear trend appears in that order parameters for methyl groups within the cytosolic cavity of M145A-bR are reduced relative to wt-bR, indicating that the mutant is less well ordered in that part so that methyl groups on average become more mobile.

Conclusion

7-TM helix proteins either transmit signals into cells indirectly via an associated protein or directly transport protons or ions across membranes. Both processes require orchestrated structural changes triggered by external stimuli. 7-TM receptors exist in a number of different sub-states,[58–60] and their mutual inter-conversion likely requires synchronized motions. With NMR spectroscopy it is possible to decipher such motional networks, and possibly even to unravel allostery.[61] Given the prevalence of methyl groups in membrane proteins, a detailed picture of side chain dynamics can be obtained from experiments that measure methyl relaxation, but these of course require methyl group assignments. Using an elaborate protocol we recently could extend assignments of bR from those determined by Patzelt *et al.* in micelles [24,62,63] to include most backbone and methyl resonances of TM portions as well.[37]

Here, we now use these methyl assignments to determine methyl group order parameter for bR in the biologically meaningful environment of lipid nanodiscs, providing a detailed picture of side chain dynamics. Methyl group order parameters have been used as proxies for conformational entropy. [57,64,65] Lee and Wand originally discovered that methyl order parameters are heterogeneously distributed and can be grouped into three major classes. [66] Using statistical methods they identified the different motional classes J, α and ω. [67] Based on their motional behavior in MD simulations, Karplus and coworkers grouped them into classes that reflect small fluctuations in a single rotamer well (high values of S^2 corresponding to the "ω-class") and those that undergo frequent rotamer transitions (low values of S^2 corresponding to the "J-class"). Recently it was discovered that methyl groups in membrane proteins are on average less well-ordered compared to soluble proteins. [55] In particular, the number of methyl groups belonging to the so-called ω-class (the most rigid methyl groups) is strongly reduced and instead a J' class is introduced for the most flexible methyl groups, which is absent in soluble proteins. In fact, in bR we could not detect any methyl group from the ω-class and similarly noticed population of the J' class, mostly by Leu methyl groups (Fig. S10). The majority of methyl groups in the internal void on the *intracellular* side of retinal belong to the α-class (high S^2) of methyl groups, indicating that this part of the protein is fairly rigid. In contrast, methyl groups on the outside of the helix bundle of bR belong to all motional classes, where also almost all methyl groups from the J' class are located. Interestingly, methyl groups with similar order parameters tend to be clustered (Fig S18). Moreover, order parameters of Ile and Leu tend to decrease with increasing distance to the retinal binding site (Fig. S13), supporting the view that bound retinal confers conformational stability to the protein center, which is propagated by allosteric pathways to the outside of the bundle. This observation agrees with recent folding studies of sensory rhodopsin using solution NMR methods that indicated that the retinal binding region constitutes the folding core of the protein.[68] Similarly, Reat et al. [69] could demonstrate higher rigidity for moieties in the retinal-binding region using elastic incoherent neutron scattering. Surprisingly, no ILV-methyl groups are present in the inside of the helix bundle at the extracellular side of bR, where 7 crystallographic water molecules are found. Instead, aromatic and polar/charged residues mainly populate this cavity.

The central process in bR activation is the isomerization of the centrally bound retinal from the all-*trans* (light-adapted) to the 13-*cis*,15-*anti* (light-activated) form upon receiving a photon.[4,7] In contrast to animal rhodopsins, this process is reversible so that retinal remains attached to bR during deactivation. Khorana and coworkers demonstrated that the 13-*cis*,15-*syn* state only 11% populated in mutant M145A-bR.[23] Interestingly, M145A-bR displayed only 10 % of the proton pumping activity of wt-bR, and isomerized retinal at reduced rates in the photocycle. Our relaxation data on the M145A-bR mutant reveal overall increased dynamics of methyl groups (Fig. S19A), in particular for residues in the cytosolic cavity (Fig. 3A), suggesting a link between conformational entropy and activity. The large 3-thiobutyl side chain of Met-145 in wt-bR packs against the β-ionone ring of retinal. Its replacement by the much smaller methyl side chain of Ala likely results in reduced ordering of atoms lining the retinal binding site which may be propagated through the protein. In that context it is notable that the all-*trans* to 13-*cis*,15-*syn* isomer ratio of the M145E mutant is very similar to wild-type, and that also the kinetics of retinal photoisomerization are almost identical.[23] We suspect that the volume of the side chain at that position influences how strongly retinal couples to the protein, and hence how the protein responds to retinal isomerization. This is also reflected in the fact that for some mutants different retinal isomers are additionally observed during photoactivation, emphasizing the pivotal role for packing of the protein against retinal. Another interesting aspect of bR biology is that retinal can also thermally isomerize to the 13-*cis*,15-*syn* form, which however, cannot directly be converted into the light-activated form by illumination.[21,49] Apparently, bR must provide sufficient structural plasticity to allow for all these structural transitions.

In our study we indirectly detected a second, much slower, conformational exchange process. Most gaps in our assignment stem from residues in the extracellular half of bR (Fig. 4A). The fact that we assigned the vast majority of observed peaks indicates that the missing resonances are broadened beyond detection by conformational exchange. Since the two isomeric forms that are present in the dark-adapted state of bR interconvert too slowly to produce the observed line-broadening,[68] we suspect that the line-broadening is rather due to motional adaptations in the extracellular cavity of bR. We speculate that those processes might be related to the exchange of internal and bulk water [70] or the lack of stabilizing contacts in the bR trimer. While we cannot fully exclude that such conformational exchange processes are absent in the trimer it is difficult to rationalize why only the extracellular portion of bR should be affected by the lack of trimer-contacts.

In this context we noticed two features common to the unassigned parts that may be related to the observed exchange-broadening effects: These are the abundance of internal water molecules and the presence of many aromatic residues in the extracellular cavity of bR (*vide infra*). The crystal structure of bR reveals that the interior is filled with 7 long-lived water molecules on the extracellular side and 2 at the intracellular side.[48] The asymmetry in the distribution of internal waters was claimed to make proton

transport unidirectional.[7] The second observation concerns the asymmetric distribution of Trp residues in the extracellular and cytosolic halves of the protein: For example, helix E (TM5) has a large number of aromatic residues, of which all tryptophan residues are located on the extracellular side (Fig. 4B, Fig. S20). Interestingly, a comparison of microbial rhodopsins revealed a large preference for tryptophan residues on the extracellular side, which is nearly as strong as the positive-inside rule [71] for Arg residues (Fig. 4C). G-protein-coupled receptors from class A and C also share this feature (Fig. S21).

Since aromatic residues strongly influence chemical shifts through the ring-current effect, changes of their rotameric states may contribute at least partially to the observed line-broadening in the extracellular part of bR. Trp residues can directly form interactions with water via hydrogen bonding to their indole Hε1 protons and hence Trp residues could play a role for reorganizing water positions. We cannot exclude that line-broadening is also related to slow motions of retinal relative to the protein. In that case, however, it is difficult to understand why these motions should only affect the extracellular half of bR.

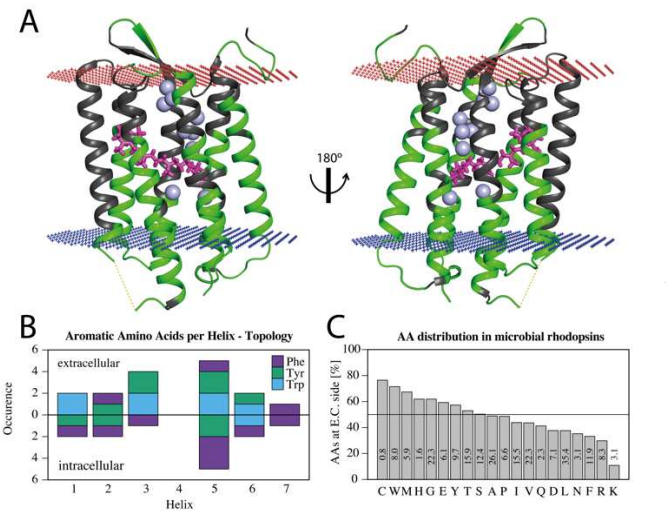

Figure 4. bR assignment and distribution of aromatic residues. A Extent of backbone assignments in bR. Residues with assigned resonances are colored in green, unassigned in black. Water molecules inside the helix bundle are depicted as blue spheres and the retinal as purple sticks. **B**. Distribution of aromatic residues in transmembrane helices in bR. **C** Relative abundance of each amino acid in the extracellular half of microbial rhodopsins (relative to the entire proteins). Bars are labeled with the average occurrence of that residue in the 36 microbial rhodopsin sequences used in the comparison.

To summarize, in the dark state we have observed dynamics on three different timescales that contribute to the function of bR: fast ns dynamics on the methyl groups that determine coupling of retinal to the protein, much slower ms dynamics likely possibly related to reorganization of the water network, and very slow dynamics to interconvert between the all-*trans* and 13-*cis*,15-*syn* states.

X-ray crystallography and recently cryo-EM are providing us, at an ever-accelerating pace, with high-resolution structures of static states of membrane proteins.[72] Indeed there are now more than 300 crystal structures reported for GPCRs. We expect that future studies on these signal transducers will focus on receptor dynamics in order to understand the trajectories of the interconversion between different states during activation and regulation. Recent XFEL studies provided molecular details of structural changes in bR after laser activation.[16] However, in that approach it was crucial to trigger the system by illumination in order to follow a *perturbed* system, a process that is not generally possible for all membrane receptors. We believe that the true potential for NMR in the field of membrane proteins is to provide data on dynamics for these difficult-to-handle receptors. The present study indicates that it is indeed possible to describe equilibrium side chain dynamics present in different conformers of the non-activated state for a 7-TM protein in nanodiscs from solution-state NMR data.

Acknowledgements

This project as support by a grant from the Swiss National Science Foundation (grant no. 310030_179314 to O.Z.) and from the Research Foundation of the University of Zurich (grant no. FK-18-083 to C.B.). We deeply thank Franz Hagn for a gift of the Δ5-MSP expression plasmid, Oksana Nekrasova for the plasmid for the BR-mistic fusion, and Fred Naider and Peter Hamm for critical reading.

Keywords: dynamics • solution NMR • rhodopsin • membrane protein • retinal isomerization

[1] U. Haupts, J. Tittor, D. Oesterhelt, *Annu. Rev. Biophys. Biomol. Struct.* **1999**, *28*, 367-399.
[2] D. Oesterhelt, *Angew. Chem. Int. Ed. Engl.* **1976**, *15*, 17-24.
[3] D. Oesterhelt, C. Bräuchle, N. Hampp, *Q. Rev. Biophys.* **1991**, *24*, 425-478.
[4] R. R. Birge, *Biochim. Biophys. Acta.* **1990**, *1016*, 293-327.
[5] R. R. Birge, *Annu. Rev. Phys. Chem.* **1990**, *41*, 683-733.
[6] L. S. Brown, O. P. Ernst, *Biochim. Biophys. Acta Proteins Proteom.* **2017**, *1865*, 1512-1521.
[7] O. P. Ernst, D. T. Lodowski, M. Elstner, P. Hegemann, L. S. Brown, H. Kandori, *Chem. Rev.* **2014**, *114*, 126-163.
[8] R. Henderson, P. N. Unwin, *Nature.* **1975**, *257*, 28-32.
[9] E. Pebay-Peyroula, G. Rummel, J. P. Rosenbusch, E. M. Landau, *Science.* **1997**, *277*, 1676-81.
[10] H. Luecke, B. Schobert, H. T. Richter, J. P. Cartailler, J. K. Lanyi, *J. Mol. Biol.* **1999**, *291*, 899-911.
[11] N. Hasegawa, H. Jonotsuka, K. Miki, K. Takeda, *Sci. Rep.* **2018**, *8*, 13123.
[12] Heberle, Fitter, Sass, Buldt, *Biophys. Chem.* **2000**, *85*, 229-248.
[13] J. Heberle, *Biochim. Biophys. Acta.* **2000**, *1458*, 135-147.
[14] T. Weinert, P. Skopintsev, D. James, F. Dworkowski, E. Panepucci, D. Kekilli, A. Furrer, S. Brünle, S. Mous, D. Ozerov, P. Nogly, M. Wang, J. Standfuss, *Science.* **2019**, *365*, 61-65.
[15] P. Nogly, T. Weinert, D. James, S. Carbajo, D. Ozerov, A. Furrer, D. Gashi, V. Borin, P. Skopintsev, K. Jaeger, K. Nass, P. Båth, R. Bosman, J. Koglin, M. Seaberg, T. Lane, D. Kekilli, S. Brünle, T. Tanaka, W. Wu, C. Milne, T. White, A. Barty, U. Weierstall, V. Panneels, E. Nango, S. Iwata, M. Hunter, I. Schapiro, G. Schertler, R. Neutze, J. Standfuss, *Science.* **2018**, *361*, eaat0094.
[16] E. Nango, A. Royant, M. Kubo, T. Nakane, C. Wickstrand, T. Kimura, T. Tanaka, K. Tono, C. Song, R. Tanaka, T. Arima, A. Yamashita, J. Kobayashi, T. Hosaka, E. Mizohata, P. Nogly, M. Sugahara, D. Nam, T. Nomura, T. Shimamura, D. Im, T. Fujiwara, Y. Yamanaka, B. Jeon, T. Nishizawa, K. Oda, M. Fukuda, R. Andersson, P. Båth, R. Dods, J. Davidsson, S. Matsuoka, S. Kawatake, M. Murata, O. Nureki, S. Owada, T. Kameshima, T. Hatsui, Y. Joti, G. Schertler, M. Yabashi, A. N. Bondar, J. Standfuss, R. Neutze, S. Iwata, *Science.* **2016**, *354*, 1552-1557.

[17] G. Nass Kovacs, J. P. Colletier, M. L. Grünbein, Y. Yang, T. Stensitzki, A. Batyuk, S. Carbajo, R. B. Doak, D. Ehrenberg, L. Foucar, R. Gasper, A. Gorel, M. Hilpert, M. Kloos, J. E. Koglin, J. Reinstein, C. M. Roome, R. Schlesinger, M. Seaberg, R. L. Shoeman, M. Stricker, S. Boutet, S. Haacke, J. Heberle, K. Heyne, T. Domratcheva, T. R. M. Barends, I. Schlichting, *Nat. Commun.* **2019**, *10*, 3177.

[18] C. R. Goldschmidt, O. Kalisky, T. Rosenfeld, M. Ottolenghi, *Biophys. J.* **1977**, *17*, 179-183.

[19] R. Govindjee, S. P. Balashov, T. G. Ebrey, *Biophys. J.* **1990**, *58*, 597-608.

[20] J. Dobler, W. Zinth, W. Kaiser, D. Oesterhelt, *Chem. Phys. Let.* **1988**, *144*, 215-220.

[21] G. S. Harbison, S. O. Smith, J. A. Pardoen, C. Winkel, J. Lugtenburg, J. Herzfeld, R. Mathies, R. G. Griffin, *Proc. Natl. Acad. Sci. U S A.* **1984**, *81*, 1706-1709.

[22] M. P. Krebs, H. G. Khorana, *J. Bacteriol.* **1993**, *175*, 1555-1560.

[23] D. A. Greenhalgh, D. L. Farrens, S. Subramaniam, H. G. Khorana, *J. Biol. Chem.* **1993**, *268*, 20305-20311.

[24] H. Patzelt, B. Simon, A. terLaak, B. Kessler, R. Kühne, P. Schmieder, D. Oesterhelt, H. Oschkinat, *Proc. Natl. Acad. Sci. U S A.* **2002**, *99*, 9765-9770.

[25] S. O. Smith, A. B. Myers, J. A. Pardoen, C. Winkel, P. P. Mulder, J. Lugtenburg, R. Mathies, *Proc. Natl. Acad. Sci. U S A.* **1984**, *81*, 2055-2059.

[26] S. O. Smith, H. J. de Groot, R. Gebhard, J. M. Courtin, J. Lugtenburg, J. Herzfeld, R. G. Griffin, *Biochemistry.* **1989**, *28*, 8897-8904.

[27] A. V. Botelho, T. Huber, T. P. Sakmar, M. F. Brown, *Biophys. J.* **2006**, *91*, 4464-4477.

[28] K. R. Rosholm, N. Leijnse, A. Mantsiou, V. Tkach, S. L. Pedersen, V. F. Wirth, L. B. Oddershede, K. J. Jensen, K. L. Martinez, N. S. Hatzakis, P. M. Bendix, A. Callan-Jones, D. Stamou, *Nat. Chem. Biol.* **2017**, *13*, 724-729.

[29] N. S. Hatzakis, V. K. Bhatia, J. Larsen, K. L. Madsen, P. Y. Bolinger, A. H. Kunding, J. Castillo, U. Gether, P. Hedegård, D. Stamou, *Nat. Chem. Biol.* **2009**, *5*, 835-841.

[30] A. Tonnesen, S. M. Christensen, V. Tkach, D. Stamou, *Biophys. J.* **2014**, *106*, 201-209.

[31] A. R. Galiakhmetov, E. A. Kovrigina, C. Xia, J. P. Kim, E. L. Kovrigin, *J. Biomol. NMR.* **2018**, *70*, 21-31.

[32] F. Hagn, M. L. Nasr, G. Wagner, *Nat. Protoc.* **2018**, *13*, 79-98.

[33] L. Frey, N. A. Lakomek, R. Riek, S. Bibow, *Angew. Chem. Int. Ed. Engl.* **2017**, *56*, 380-383.

[34] I. Kucharska, T. C. Edrington, B. Liang, L. K. Tamm, *J. Biomol. NMR.* **2015**, *61*, 261-274.

[35] L. Sušac, R. Horst, K. Wüthrich, *ChemBioChem.* **2014**, *15*, 995-1000.

[36] P. Ma, J. Mohrlüder, M. Schwarten, M. Stoldt, S. K. Singh, R. Hartmann, V. Pacheco, D. Willbold, *ChemBioChem.* **2010**, *11*, 1967-1970.

[37] L. Kooijman, P. Ansorge, M. Schuster, C. Baumann, F. Löhr, S. Jurt, P. Güntert, O. Zerbe, *J. Biomol. NMR.* **2020**, *74*, 45-60.

[38] E. Schmidt, P. Güntert, *J. Am. Chem. Soc.* **2012**, *134*, 12817-12829.

[39] I. Pritišanac, J. M. Würz, T. R. Alderson, P. Güntert, *Nat. Commun.* **2019**, *10*, 4922.

[40] O. V. Nekrasova, A. N. Wulfson, R. V. Tikhonov, S. A. Yakimov, T. N. Simonova, A. I. Tagvey, D. A. Dolgikh, M. A. Ostrovsky, M. P. Kirpichnikov, *J. Biotechnol.* **2010**, *147*, 145-150.

[41] Y. Sugiyama, Y. Mukohata, *J. Biochem.* **1996**, *119*, 1143-1149.

[42] F. Hagn, M. Etzkorn, T. Raschle, G. Wagner, *J. Am. Chem. Soc.* **2013**, *135*, 1919-1925.

[43] I. G. Denisov, Y. V. Grinkova, A. A. Lazarides, S. G. Sligar, *J. Am. Chem. Soc.* **2004**, *126*, 3477-3487.

[44] V. Tugarinov, L. E. Kay, *J. Am. Chem. Soc.* **2003**, *125*, 13868-13878.

[45] P. Scherrer, M. K. Mathew, W. Sperling, W. Stoeckenius, *Biochemistry.* **1989**, *28*, 829-834.

[46] N. A. Dencher, M. P. Heyn, *FEBS Lett.* **1979**, *108*, 307-310.

[47] N. A. Dencher, K. D. Kohl, M. P. Heyn, *Biochemistry.* **1983**, *22*, 1323-1334.

[48] B. Schobert, J. Cupp-Vickery, V. Hornak, S. Smith, J. Lanyi, *J. Mol. Biol.* **2002**, *321*, 715-726.

[49] T. Nishikawa, M. Murakami, T. Kouyama, *J. Mol. Biol.* **2005**, *352*, 319-328.

[50] N. A. Lakomek, J. Ying, A. Bax, *J. Biomol. NMR.* **2012**, *53*, 209-221.

[51] D. Sheppard, R. Sprangers, V. Tugarinov, *Prog. Nucl. Magn. Reson. Spectrosc.* **2010**, *56*, 1-45.

[52] H. Sun, L. E. Kay, V. Tugarinov, *J. Phys. Chem. B.* **2011**, *115*, 14878-14884.

[53] V. Tugarinov, R. Sprangers, L. E. Kay, *J. Am. Chem. Soc.* **2007**, *129*, 1743-1750.

[54] T. I. Igumenova, K. K. Frederick, A. J. Wand, *Chem. Rev.* **2006**, *106*, 1672-1699.

[55] E. S. O'Brien, B. Fuglestad, H. J. Lessen, M. A. Stetz, D. W. Lin, B. S. Marques, K. Gupta, K. G. Fleming, A. J. Wand, *Angew. Chem. Int. Ed. Engl.* **2020**, *59*, 11108-11114.

[56] K. A. Sharp, *Meth. Enzymol.* **2019**, *615*, 1-39.

[57] A. J. Wand, K. A. Sharp, *Annu. Rev. Biophys.* **2018**, *47*, 41-61.

[58] A. J. Venkatakrishnan, X. Deupi, G. Lebon, C. G. Tate, G. F. Schertler, M. M. Babu, *Nature.* **2013**, *494*, 185-194.

[59] B. Kobilka, *Angew. Chem. Int. Ed. Engl.* **2013**, *52*, 6380-6388.

[60] T. Flock, A. S. Hauser, N. Lund, D. E. Gloriam, S. Balaji, M. M. Babu, *Nature.* **2017**, *545*, 317-322.

[61] G. P. Lisi, K. W. East, V. S. Batista, J. P. Loria, *Proc. Natl. Acad. Sci. U S A.* **2017**, *114*, E3414-E3423.

[62] H. Patzelt, A. S. Ulrich, H. Egbringhoff, P. Dux, J. Ashurst, B. Simon, H. Oschkinat, D. Oesterhelt, *J. Biomol. NMR.* **1997**, *10*, 95-106.

[63] M. Schubert, M. Kolbe, B. Kessler, D. Oesterhelt, P. Schmieder, *ChemBioChem.* **2002**, *3*, 1019-1023.

[64] V. Kasinath, K. A. Sharp, A. J. Wand, *J. Am. Chem. Soc.* **2013**, *135*, 15092-15100.

[65] E. S. O'Brien, A. J. Wand, K. A. Sharp, *Protein Sci.* **2016**, *25*, 1156-1160.

[66] A. L. Lee, A. J. Wand, *Nature.* **2001**, *411*, 501-504.

[67] K. A. Sharp, V. Kasinath, A. J. Wand, *Proteins.* **2014**, *82*, 2106-2117.

[68] Y. L. Tan, J. Mitchell, J. Klein-Seetharaman, D. Nietlispach, *J. Mol. Biol.* **2019**, *431*, 2790-2809.

[69] V. Réat, H. Patzelt, M. Ferrand, C. Pfister, D. Oesterhelt, G. Zaccai, *Proc. Natl. Acad. Sci. U S A.* **1998**, *95*, 4970-4975.

[70] O. Edholm, O. Berger, F. Jähnig, *J. Mol. Biol.* **1995**, *250*, 94-111.

[71] G. von Heijne, *J. Mol. Biol.* **1992**, *225*, 487-494.

[72] R. Grisshammer, *Protein Sci.* **2017**, *26*, 1493-1504.

10.1002/anie.202004393

Entry for the Table of Contents

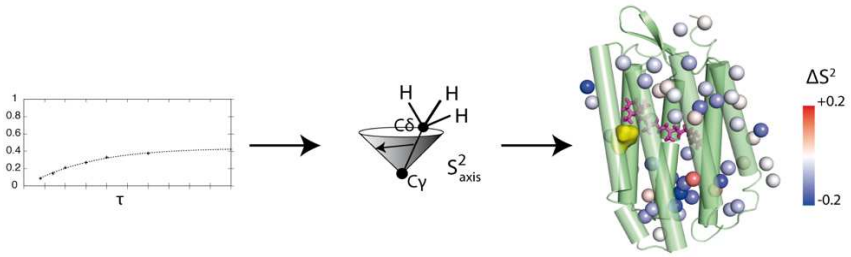

Dynamics of sidechains are probed in bacteriorhodopsin and a less active mutant from NMR measurements of methyl relaxation.

Institute and/or researcher Twitter usernames: @ZerbeOliver